Journal of Hazardous Materials 217–218 (2012) 231–237

Contents lists available at SciVerse ScienceDirect

Journal of Hazardous Materials

journal homepage: www.elsevier.com/locate/jhazmat

Visible-light photocatalytic inactivation of *Escherichia coli* by $K_4Nb_6O_{17}$ and Ag/Cu modified $K_4Nb_6O_{17}$

Hsin-yu Lin [a,*], Hong-mou Lin [b]

[a] Department of Materials Science and Engineering, National Dong Hwa University, Hualien 974, Taiwan
[b] Department of Chemistry, National Dong Hwa University, Hualien 974, Taiwan

ARTICLE INFO

Article history:
Received 19 December 2011
Received in revised form 20 February 2012
Accepted 6 March 2012
Available online 14 March 2012

Keywords:
$K_4Nb_6O_{17}$
Photocatalyst
Ag–Cu cocatalyst
Antibacteria

ABSTRACT

Ag/Cu modified $K_4Nb_6O_{17}$ thin film, a novel type of photocatalyst for photocatalytic inactivation of *Escherichia coli* under visible light irradiation was developed. The effects of loading method of Cu species on the characteristics of Ag–Cu nanocomposites and photocatalytic antibacterial activity were studied. Samples were characterized by powder X-ray diffraction (XRD), transmission electron microscopy (TEM), X-ray photoelectron spectroscopy (XPS) and ultraviolet–visible spectroscopy (UV–Vis). Irrespective of the preparation method, loading Ag, Cu and Ag–Cu composite as cocatalyst led to an increase in antibacterial activity as compared to bare $K_4Nb_6O_{17}$. In comparison with conventional impregnation method, well dispersed Ag–Cu nanocomposites were obtained on the $K_4Nb_6O_{17}$ surface by a sodium borohydride reduction method in the presence PVP. In this case, markedly improvement of photocatalytic activity was observed. The significant enhancement was ascribed to the high efficiency of electron hole pair separation related to the Ag–Cu nanocomposite on $K_4Nb_6O_{17}$ surface and the synergistic effects of coexisting Ag and Cu ions on antibacterial activity.

1. Introduction

Our world is always under threat from biological contamination. Recent outbreaks of virulent *Escherichia coli* contamination in Germany have demonstrated the urgent need worldwide to control the harmful pathogen. Developing a photocatalytic system for antibacterial control using light is a topic of great interest, and is of fundamental as well as practical importance. The photocatalytic deactivation of microorganisms is a cheap, clean and safe alternative as compared to chemical disinfections such as chlorine, iodine and ozone treatment. When a semiconductor photocatalyst is illuminated with photons with energies greater than its band gap, electron–hole pairs are generated due to photo-excitation. Highly oxidative hydroxyl radicals are generated by the oxidation of water at the valence band of semiconductor photocatalyst whose valence band level is more positive than the oxidation potential of H_2O. Further, oxygen is reduced to reactive oxygen species such as superoxide anion and hydrogen peroxide by the photo excited electrons of the photocatalyst whose conduction band edge should be more negative than the reduction potential of O_2 [1]. Although the mechanism of antibacterial action has not been fully elucidated, it is believed that the reactive oxygen species produced by the photocatalytic reactions cause various damages to microorganisms [2,3].

As it is well known, titanium oxide is the most widely used photocatalyst for wastewater treatment and destruction of volatile organic compounds. TiO_2 photocatalyst has also shown to be effective for bacterial inactivation under UV light irradiation. However, the incoming solar energy contains only about 4% UV energy. On the other hand, exposure to UV light would cause damage to human skin [4]. Hence, applications of photocatalytic disinfection driven by UV light are significantly limited. Many studies have been made to develop highly efficient photocatalysts for bacterial inactivation driven by visible light. Yu et al. [5] reported that sulfur-doped titanium dioxide showed visible-light induced photokilling capability on *Micrococcus lylae* (gram-positive) cells where the survival ratio of *M. lylae* decreased to 3.3% after 60 min irradiation. Recently, Wu et al. [6] reported that the combination of Ag_2O and TiON photocatalysts showed high efficiency on the photokilling of *E. coli* (gram-negative) in a suspension photoreactor.

Furthermore, the activity of photocatalyst could be improved by loading cocatalyst, such as Pt, Cu, Ag, and ZnO [7–9]. Tseng et al. [7] reported that significant enhancement effects of loading Cu on TiO_2 for the photoreduction of CO_2. Page et al. [10] reported that Ag modified TiO_2 was significantly more photocatalytically and antimicrobially active than TiO_2. In addition, silver ion is known as a good antibacterial agent [15,16]. Silver sulfadiazine cream is one of the most widely used for the managing burns [11]. Ag ions can

* Corresponding author.
E-mail address: hsinyu@mail.ndhu.edu.tw (H.-y. Lin).

0304-3894/$ – see front matter © 2012 Elsevier B.V. All rights reserved.
doi:10.1016/j.jhazmat.2012.03.014

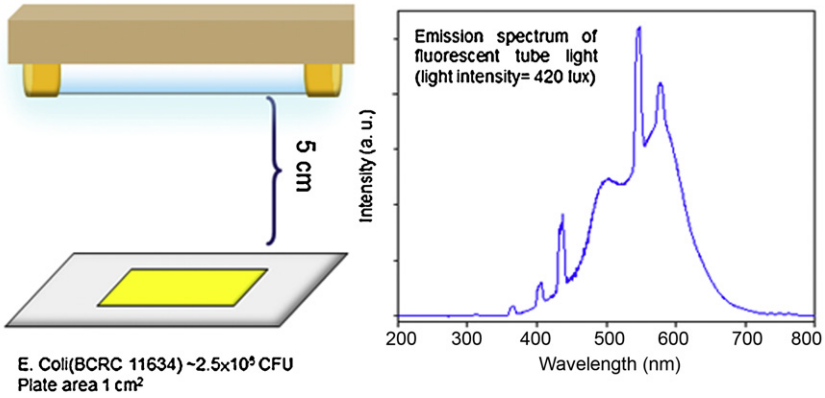

Fig. 1. Schematic diagram of antibacterial test.

interact with the thiol groups in protein and subsequently inactivated of key enzymes. Also, Ag ions could kill bacteria by denaturing their DNA molecular [12]. Several comprehensive reviews have reported on the aspects of the disinfection mechanisms [13] and photocatalytic antibacterial mechanisms [14].

On the other hand, much effort has been devoted to studying the photocatalytic properties of transition metal oxides with a d^0 electron configuration such as $InNi_{0.1}TaO_4$ [15], $K_4Nb_6O_{17}$ [16,17], and $BiVO_4$ [18] for hydrogen production from water splitting under visible light irradiation. Nevertheless, very few studies have investigated the photocatalytic disinfection of non-TiO_2 photocatalysts. Previously, our group had reported that highly crystalline single phase $K_4Nb_6O_{17}$ can be prepared by a two-step solid-state reaction process and showed photocatalytic activity for water splitting under visible light [16]. $K_4Nb_6O_{17}$ consists of four layers of NbO_6 orthorhombic units where the anisotropic niobate sheets stacked along the b axis form two types of interlayer regions, which are denoted by Interlayer I and Interlayer II [19]. $K_4Nb_6O_{17}$ may be a good candidate for photocatalytic disinfection under visible light due to its anisotropic layered structure for efficient charge separation.

In the present study, we present a series of novel $K_4Nb_6O_{17}$ thin film photocatalysts with Ag, Cu, Ag–Cu cocatalysts for photocatalytic disinfection under visible light irradiation. Individual and combined effects of Cu and Ag cocatalysts on $K_4Nb_6O_{17}$ were investigated. Special attention has been focused on the effects on the relationship between loading method of Ag–Cu nanoparticles and photocatalytic disinfection activity. The catalysts were studied using powder X-ray diffraction (XRD), transmission electron microscopy (TEM), ultraviolet–visible spectroscopy (UV–Vis), scanning electron microscopy–energy dispersive X-ray spectrometer (SEM–EDX) and X-ray photoelectron spectroscopy (XPS). The antibacterial activity of photocatalyst film was evaluated under the Japanese standard JIS Z 2801: 2006 [20].

2. Experimental

The preparation of $K_4Nb_6O_{17}$ catalysts were synthesized by a two-step solid-state reaction (SSR) using K_2CO_3 and Nb_2O_5 with 99.99% purity (molar ratio 2.1:3). The mixed precursor was calcined in air at 1073 K for 5 h then at 1273 K for 5 h with an intermediate grinding process between the two calcinations.

The Ag–$K_4Nb_6O_{17}$, Cu–$K_4Nb_6O_{17}$ catalyst was prepared by loading 1 wt% Ag and 1 wt% Cu on $K_4Nb_6O_{17}$ powders using aqueous $AgNO_3$ and $Cu(NO_3)_2$ solution, respectively.

Ag–Cu(1) $K_4Nb_6O_{17}$ catalyst was prepared by loading 0.5% Ag and 0.5 wt% Cu on $K_4Nb_6O_{17}$. Distilled water containing an appropriate amount of $AgNO_3$ and $Cu(NO_3)_2$ was premixed before the impregnation process. Following the impregnation process, the film of Ag–$K_4Nb_6O_{17}$, Cu–$K_4Nb_6O_{17}$ and Ag–Cu(1) $K_4Nb_6O_{17}$ was prepared with the same protocol as following: 0.15 g photocatalyst was dispersed in 1 ml of distilled water to make a slurry and subsequently coated on glass substrate via a doctor-blade method with an active area about 1 cm^2. The film was dried for 30 min on a hot plate at 80 °C and subsequently calcined at 400 °C for 70 min.

Ag–Cu(2) $K_4Nb_6O_{17}$ and Ag–Cu(3) $K_4Nb_6O_{17}$ catalyst were prepared by loading 0.5 wt% Cu on $K_4Nb_6O_{17}$ by dissolving appropriate amount of $CuSO_4{\cdot}5H_2O$ in 25 ml of distilled water where 0.7 g PVP (polyvinyl pyrrolidone, M_{av} = 55,000) had previously been added. The mixture was stirred under nitrogen for 20 min. Then, 25 ml 0.01 M aqueous solution of sodium borohydride was added to the solution and further reacted under nitrogen for 20 min. After centrifugation and washing, the resulting product was dried at 60 °C overnight. Subsequently, 0.5 wt% Ag was loaded on the product by impregnation process. The film was prepared by the same protocol as described above. The Ag–Cu(2) $K_4Nb_6O_{17}$ film was referred as the sample before calcination. After calcined at 400 °C for 70 min, the sample was denoted as Ag–Cu(3) $K_4Nb_6O_{17}$. The Cu and Ag loading were measured by inductively coupled plasma mass spectrometry (ICP-MS, see Supplementary data).

The characterization methods included powder X-ray diffraction (XRD, Cu Kα radiation, λ = 1.54178 Å), TEM (JEOL JEM-2000FX Π microscope), SEM/EDS (Hitachi S-3500H), and UV–Vis (Varian Lary 5E diode array spectrometer). The XPS spectra were recorded with a VG Scientific ESCALAB 250. The binding energy of XPS were corrected by contaminant carbon (C_{1s} = 284.6 eV) in order to facilitate the comparisons of the values among the catalysts and the standard compounds.

The antibacterial activity of photocatalyst film was evaluated under the Japanese standard JIS Z 2801: 2006 [20]. *E. coli* (BCRC 11634) was incubated in Luria–Bertani (LB) broth at 37 °C for 12–16 h at relative humidity ≥95%. The *E. coli* was grown to $1–3 \times 10^9$ colony-forming units (CFU/ml) which was determined by the spectroscopy enumeration method, and then the cell suspension was diluted to about 1.0×10^7 to 5.0×10^7 CFU/ml in LB broth. 50 μl of cell suspension (about 2.5×10^6 CFU) was then plated on the sample specimens. The samples were illuminated by two 10 W fluorescent tube light (China Electric MFG. Corporation, FL10D, 420 lux) for 45 min as shown in Fig. 1. Specimens on glass substrate without photocatalyst were carried out as control experiments. The sample specimens treated by the same protocol with no light irradiation was used as dark control experiments. All the photocatalytic experiments were repeated three times. The antibacterial test was effective while: (i) $(\log(N_{max}) - \log(N_{min}))/\log(N_{avg}) \leq 0.2$, where N_{max}, N_{min}, and N_{avg} was the maximum, minimum and average number of viable cells, respectively. (ii) The average of the

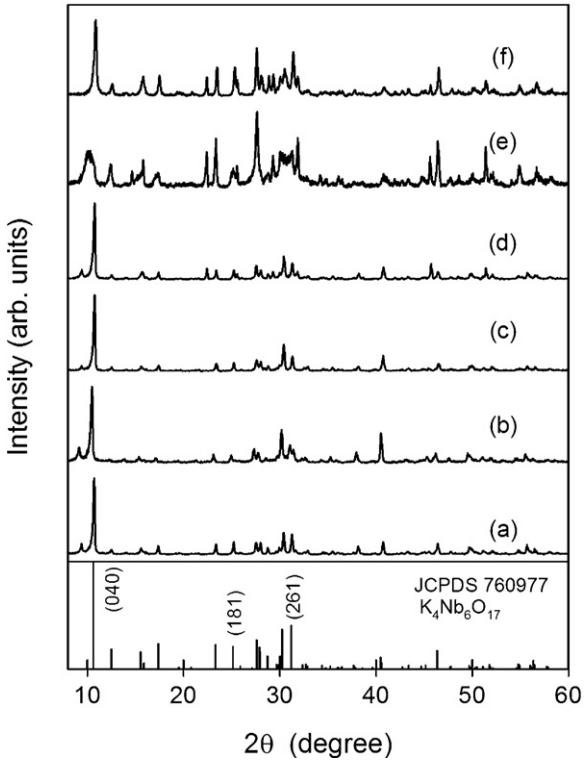

Fig. 2. XRD patterns of (a) $K_4Nb_6O_{17}$, (b) Ag–$K_4Nb_6O_{17}$, (c) Cu–$K_4Nb_6O_{17}$, (d) Ag–Cu(1) $K_4Nb_6O_{17}$, (e) Ag–Cu(2) $K_4Nb_6O_{17}$ and (f) Ag–Cu(3) $K_4Nb_6O_{17}$.

number of viable cells of bacteria after reaction on untreated specimens should between 1 and 4×10^5 CFU. Then, the survival fraction of *E. coli* was calculated as following: survival fraction of *E. coli* (%) = N_a/N_b where N_a is the number of viable cells on the antimicrobial specimens and N_b is the number of viable cells on the untreated specimens.

3. Results and discussion

The layered structure of $K_4Nb_6O_{17}$ belong to orthorhombic group $P21nb$ (33), $a = 7.830$ Å, $b = 3.321$ Å, $c = 6.46$ Å where the $[Nb_6O_{17}]^{4-}$ layered structures are composed of corner-sharing NbO_6 octahedral units [19]. Fig. 2(a) shows the XRD pattern of the $K_4Nb_6O_{17}$ catalyst prepared by two step solid-state reaction which are well consisted with the lamellar potassium niobate, $K_4Nb_6O_{17}$ (JCPDS 76-0977), indicating that the samples were fully crystallized orthorhombic $K_4Nb_6O_{17}$. Fig. 2(b)–(d) shows the XRD patterns of a series of $K_4Nb_6O_{17}$ samples modified with Ag and Cu species by impregnation method. The XRD patterns of all samples were identical to $K_4Nb_6O_{17}$ sample. The sharp diffraction peak observed around at $2\theta = 10.7^\circ$ ($d_{040} = 8.3$ Å) indicated that these samples were fully crystallized orthorhombic anhydrous $K_4Nb_6O_{17}$ [19]. The results indicated that no significant crystalline distortion of $K_4Nb_6O_{17}$ was induced by loading Ag and Cu species. However, the XRD pattern of Ag–Cu(2)–$K_4Nb_6O_{17}$ (Fig. 2(e)) catalyst shows a peak broadening, and decreased intensity of the (0 4 0) diffraction peak. The decreased peak intensity and peak broadening of the $K_4Nb_6O_{17}$ (0 4 0) peak indicating the structural distortion of $K_4Nb_6O_{17}$ induced by copper reduction with sodium borohydride. Bizeto et al. [21] reported that the basal spacing value of (0 4 0) peak of $K_4Nb_6O_{17}$ increased to 9.48 Å when three water molecules was intercalated in the layer structure of $K_4Nb_6O_{17}$. Thus, the (0 4 0) peak shift of Ag–Cu(2)–$K_4Nb_6O_{17}$ catalyst was attributed by the water intercalation in $K_4Nb_6O_{17}$. This can be further proved by the sharp (0 4 0) peak appeared at $2\theta = 10.8^\circ$ in XRD pattern of Ag–Cu(3)–$K_4Nb_6O_{17}$ which was due to the release of intercalated water in $K_4Nb_6O_{17}$. In addition, the sharp (0 4 0) peak indicated that calcination at 400 °C could effectively increase the crystallinity of Ag–Cu(3)–$K_4Nb_6O_{17}$ catalyst.

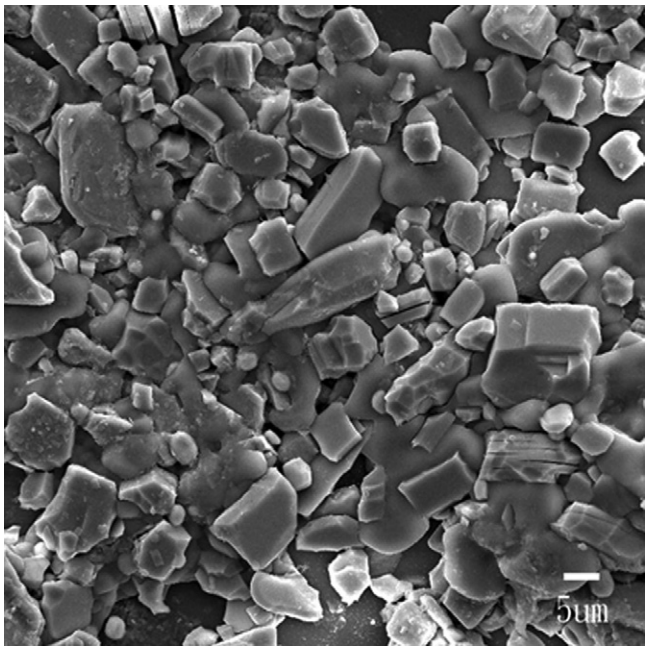

Fig. 3. SEM image of Ag–Cu(1) $K_4Nb_6O_{17}$ film.

Fig. 3 shows the SEM image of Ag–Cu(1) $K_4Nb_6O_{17}$ film, the high temperature solid-state synthesis caused the formation of large $K_4Nb_6O_{17}$ particle with a diameter of 1–10 μm. Fig. 4(a) shows the TEM image of Ag–$K_4Nb_6O_{17}$ catalyst where large Ag particles (>50 nm) were observed on the particle edge of $K_4Nb_6O_{17}$. This suggests that Ag precursor could migrate easily along the particle edge of $K_4Nb_6O_{17}$, and form large aggregates. On the other hand, the TEM image of Ag–Cu(3) $K_4Nb_6O_{17}$ catalyst (see inset of Fig. 4(b)) revealed clearly that Ag–Cu composite formed a narrow particle distribution with a mean particle size of 12 nm on the particle edge of $K_4Nb_6O_{17}$. Moreover, no large aggregate was observed. Although it is difficult to form ultrafine metal particles on a well-crystallized large particle with small surface area and smooth surface than a porous or small particle [22], Ag–Cu nanocomposite cocatalysts with a mean particle size of 12 nm on $K_4Nb_6O_{17}$ surface was successfully synthesized by a two steps process. First, the copper nanoparticle was loaded on the $K_4Nb_6O_{17}$ surface by reduction method by using sodium borohydride as reduction agent and PVP as polymeric anti-agglomerate [23]. Followed the reduction reaction, Ag was impregnated to the sample. Our results demonstrated that after further calcination at 400 °C, no considerable aggregation of Ag–Cu nano-composites was occurred.

The UV–Vis spectra of Ag and Cu modified $K_4Nb_6O_{17}$ catalysts are shown in Fig. 5. The band gap of the $K_4Nb_6O_{17}$ catalyst in this study was about 3.3 eV, as estimated from the UV–Vis spectrum. It can be seen that a red-shift of absorption edge was observed in the UV–Vis spectra of Ag and Cu modified $K_4Nb_6O_{17}$ catalysts. The red-shift of the adsorption edges for nickel modified $K_4Nb_6O_{17}$ phototatalyst has been reported previously [16], which was evident as an important influence for visible light absorption and the photocatalytic property. In Fig. 4(a) and (b) we can see that Ag–$K_4Nb_6O_{17}$ catalyst displays a similar UV–Vis absorption as $K_4Nb_6O_{17}$ where only a small absorption increase can be observed at about 360 nm. This result was similar to Ag/TiO_2 prepared by impregnation method [24].

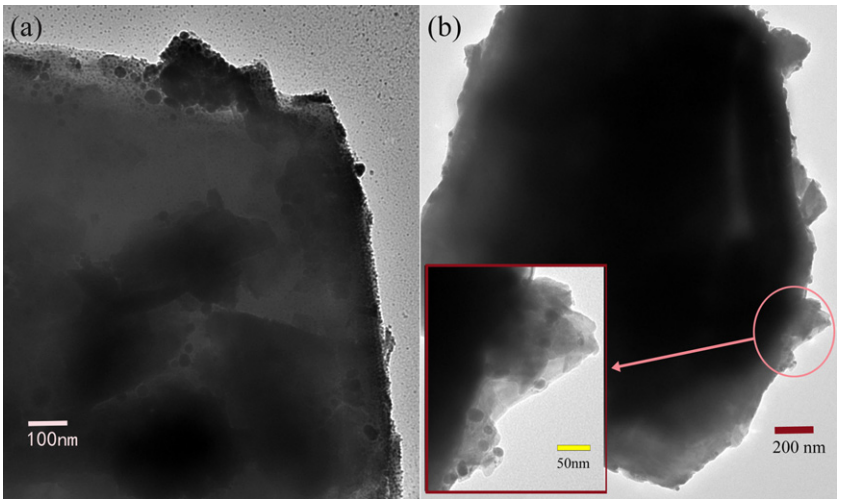

Fig. 4. TEM images of (a) Ag–$K_4Nb_6O_{17}$ and (b) Ag–Cu(3) $K_4Nb_6O_{17}$ photocatalysts.

On the other hand, the Cu–$K_4Nb_6O_{17}$ catalyst shows a new absorption shoulder at 350–500 nm. As reported by Tseng and Wu [9], red-shift of the absorption edges was obtained in the UV–Vis spectra of 2 wt% Cu/TiO_2 photocatalyst where copper served as an electron trap to reduce the recombination rate of photo exited electron–hole pairs and promoted photocatalytic CO_2 reduction for methanol production. Similar characteristic absorptions at long wavelengths were also observed in the UV–Vis spectra of Ag–Cu(1) $K_4Nb_6O_{17}$ and Ag–Cu(2) $K_4Nb_6O_{17}$ suggested that it was attributed to Cu species on $K_4Nb_6O_{17}$ surface. Fig. 6 shows the XPS spectra and film appearances of Ag–Cu modified $K_4Nb_6O_{17}$ catalysts via different preparation process. The Cu species of Ag–Cu(1) $K_4Nb_6O_{17}$ catalyst can be identified from the Cu $2p_{3/2}$ peak at 933.0 eV Cu $2p_{1/2}$ peak at 953.5 eV and their satellite peak at 943.0 eV and 962.5 eV [25]. Also, it can be seen that the color of Ag–Cu(1) $K_4Nb_6O_{17}$ film was black. The Cu $2p_{3/2}$ peaks of Ag–Cu(2) $K_4Nb_6O_{17}$ and Ag–Cu(3) $K_4Nb_6O_{17}$ catalysts appeared at 932.6 eV and no satellite peaks can be found, indicating the Cu species were Cu^0 or Cu^+. From Fig. 6, one can see that the color of Ag–Cu(2) $K_4Nb_6O_{17}$ was light orange and it was changed to dull brown after subsequently calcination. Hence, although it was difficult to discriminate between Cu^0 and Cu^+ species by Cu $2p_{3/2}$ and Cu $2p_{1/2}$ peaks because their binding energies are very close [25], the color of the films suggested that the Cu species of Ag–Cu(2) $K_4Nb_6O_{17}$ was major metallic copper with minor Cu^+ species and the main Cu species of Ag–Cu(3) $K_4Nb_6O_{17}$ was Cu_2O.

Similar to Ag–TiO_2 prepared by impregnation method, the color of Ag–$K_4Nb_6O_{17}$ was light gray indicated the metallic nature of Ag nanoparticles [26]. It should be noticed that because the valence states of Ag^0 and Ag^+ are closely spaced and the significant overlapping with the Nd 3p BE at 365–375 eV [27], it was not able to identify silver states on $K_4Nb_6O_{17}$ from XPS measurements. According to the color of the films, the main Ag states of calcined $K_4Nb_6O_{17}$ samples (Ag–$K_4Nb_6O_{17}$, Ag–Cu(1) $K_4Nb_6O_{17}$, and Ag–Cu(3) $K_4Nb_6O_{17}$)

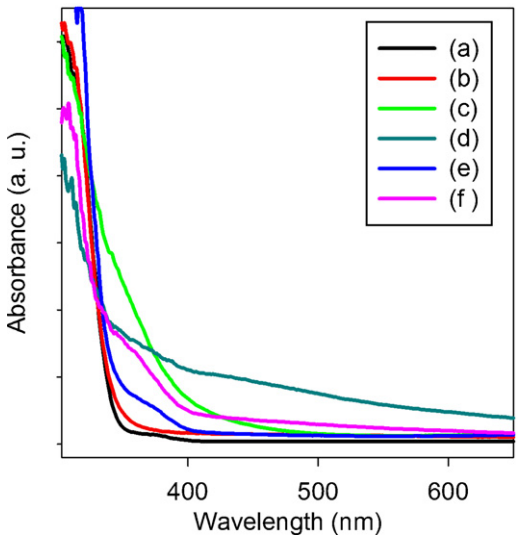

Fig. 5. UV–Vis spectra of (a) $K_4Nb_6O_{17}$, (b) Ag–$K_4Nb_6O_{17}$, (c) Cu–$K_4Nb_6O_{17}$, (d) Ag–Cu(1) $K_4Nb_6O_{17}$, (e) Ag–Cu(2) $K_4Nb_6O_{17}$ and (f) Ag–Cu(3) $K_4Nb_6O_{17}$.

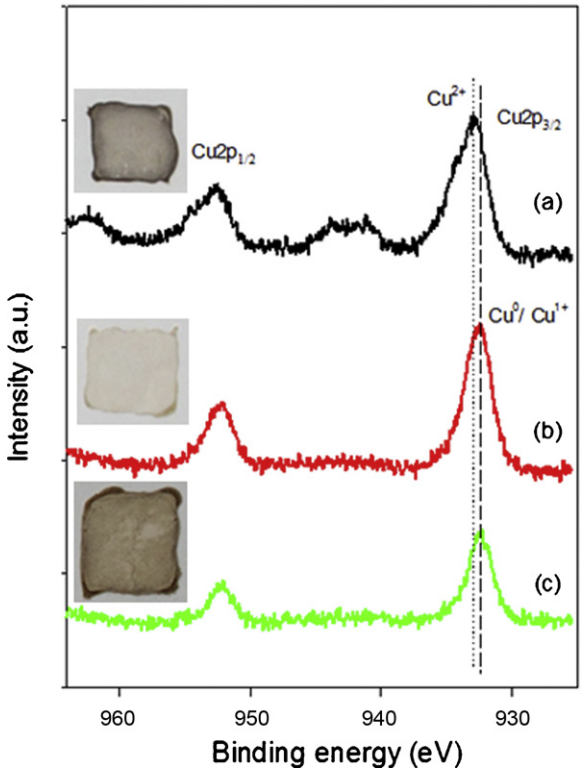

Fig. 6. XPS spectra of Cu_{2p} states and appearances of (a) Ag–Cu(1)–$K_4Nb_6O_{17}$, (b) Ag–Cu(2) $K_4Nb_6O_{17}$ and (c) Ag–Cu(3) $K_4Nb_6O_{17}$ films.

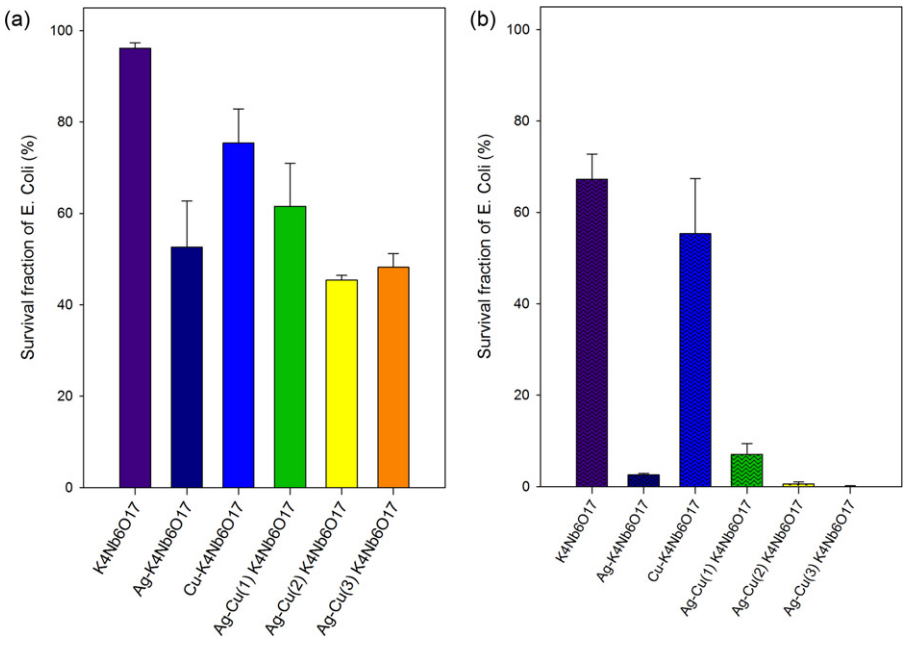

Fig. 7. The antibacterial efficiency of *E. coli* on $K_4Nb_6O_{17}$, Ag–$K_4Nb_6O_{17}$, Cu–$K_4Nb_6O_{17}$ and Ag–Cu(n) $K_4Nb_6O_{17}$ (n = 1–3) photocatalysts. The antibacterial test was carried out (a) in dark and (b) under visible light irradiation for 45 min.

should be Ag_2O coexistence with metallic Ag [24] while the main Ag species of Ag–Cu(2) $K_4Nb_6O_{17}$ was Ag^+ ions.

The antibacterial efficiency of *E. coli* on Ag, Cu, and Ag–Cu modified $K_4Nb_6O_{17}$ thin films were studied in dark and under visible light irradiations, as shown in Fig. 7. It is known that metals such as Ag, Cu affect thiol groups in protein and subsequently inactivated microbial metabolism [13,28]. Lin et al. [29] reported that Cu ions could destroy cell wall permeability and Ag ions could kill bacteria by denaturing enzymes. Both Cu and Ag ions were antibacterial effective against *Legionella pneumophila*. The combination of Cu and Ag ions showed a synergy effect which enhanced the inactivation of *L. pneumophila*. Fig. 6a demonstrated the intrinsic antibacterial activity of samples. The Ag–$K_4Nb_6O_{17}$ exhibited a better antibacterial activity of *E. coli* than Cu–$K_4Nb_6O_{17}$ in dark as reported by Ruparelia et al. [30]. It should be noticed that even with a lower Ag content, Ag–Cu(2) $K_4Nb_6O_{17}$ and Ag–Cu(3) $K_4Nb_6O_{17}$ presented a better antibacterial activity of *E. coli* than Ag–$K_4Nb_6O_{17}$. The superior antibacterial properties were attributed to the well dispersed Ag–Cu nanocomposite cocatalysts on $K_4Nb_6O_{17}$ prepared by $NaBH_4$ reduction in the presence of PVP. It provided more active sites for bacterial adsorption and released Ag and Cu ions to LB medium more efficiently which enhancing the synergy effect of antibacterial activity [30] than Ag–Cu(2) $K_4Nb_6O_{17}$ prepared by conventional impregnation method.

As shown in Fig. 7, the survival of *E. coli* on $K_4Nb_6O_{17}$ film was more than 90% in dark, and decreased to 67% under visible light irradiation indicated that the reduction of viable bectieria on $K_4Nb_6O_{17}$ was photocatalytic. Under visible light irradiation, the antibacterial activity of *E. coli* was significantly improved by loading Ag, which indicated an efficient electron–hole separation of Ag–$K_4Nb_6O_{17}$ [31]. Although the UV–Vis of Cu–$K_4Nb_6O_{17}$ film showed a strong absorption in long wavelength region, the photocatalytic antibacterial activity of Cu–$K_4Nb_6O_{17}$ was relatively low as compared to Ag modified samples. This might due to the lower intrinsic antibacterial activity of Cu ions and the suppression of electron–hole recombination by CuO was not as efficient as AgO_x. Both Ag–Cu(2)/$K_4Nb_6O_{17}$ and Ag–Cu(3)/$K_4Nb_6O_{17}$ photocatalysts prepared by reduction method showed excellent antimicrobial property which eliminated >99% of bacteria in 45 min where Ag–Cu(3)/$K_4Nb_6O_{17}$ catalyst exhibited the best antimicrobial activity.

Although it is believed that the reactive oxygen species produced by the photocatalytic reactions causing damages of bacterial cell, there were several mechanism proposed to describe the photokilling process of *E. coli*. Pal et al. [32] reported a first order photocatalytic inactivation model of *E. coli* on TiO_2 under UV-A irradiation. Sunada et al. [33] demonstrated a two-step mechanism for photokilling of *E. coli* of TiO_2 film under UV light illumination. To further understand the photokilling process of *E. coli* on $K_4Nb_6O_{17}$, the antibacterial tests with respect to time under visible light irradiation were carried out. Fig. 8 shows the photographs of time-titration antibacterial experiments on Ag–Cu(3) $K_4Nb_6O_{17}$ where >99% of *E. coli* was destroyed in 30 min. Furthermore, Fig. 9 shows the survival fraction of a series Ag modified $K_4Nb_6O_{17}$ present in this study. After 5 min irradiation under visible light, obvious changes in survival were observed on Ag–$K_4Nb_6O_{17}$ and Ag–Cu(3) $K_4Nb_6O_{17}$ where the survival fraction of *E. coli* decreased to 67% and 51%, respectively. These results indicated that the electron–hole separation was hindered by Ag which enhanced the production of reactive oxygen species and destroyed the cell wall and outer membrane of *E. coli*. Therefore, the Ag ions could permeate into the cell efficiently and inactivated the proteins. The superior photokilling ability of Ag–Cu(3) $K_4Nb_6O_{17}$ than Ag–$K_4Nb_6O_{17}$ indicated that Cu species within Ag–Cu nanocomposite cocatalysts provided a more benefit chemical environment than Ag nanoparticles for photocatalytic bacterial inactivation. On the contrary, only a small fraction of *E. coli* was killed on Ag–Cu(1) $K_4Nb_6O_{17}$ and Ag–Cu(2) $K_4Nb_6O_{17}$ photocatalysts at the beginning, and then the reaction rate was increased. It suggested that the reactive oxygen species was insufficient to disorder the outer membrane of *E. coli* and exhibited a two-step photokilling dynamics. Based on these observations, the photocatalytic inactivation of *E. coli* on Ag–Cu modified $K_4Nb_6O_{17}$ was affected by complex factors including loading amount, particle size, and chemical states of the cocatalysts, and further investigation was required.

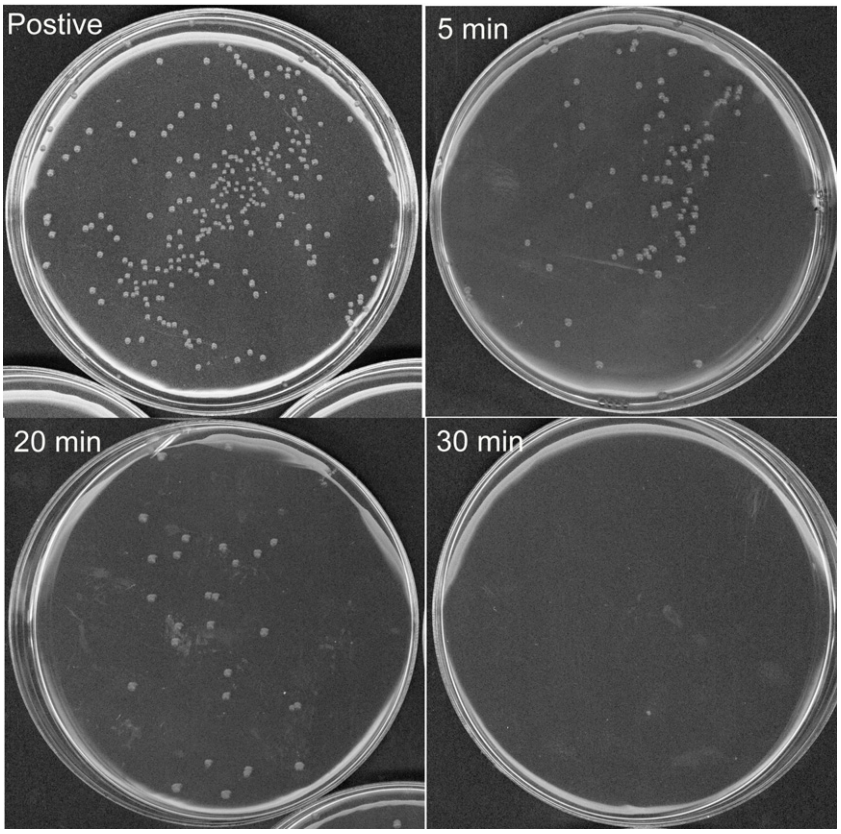

Fig. 8. Photographs of time-titration antibacterial experiments on Ag–Cu(3) $K_4Nb_6O_{17}$ catalyst under visible light irradiation (positive control: specimen without coating photocatalyst).

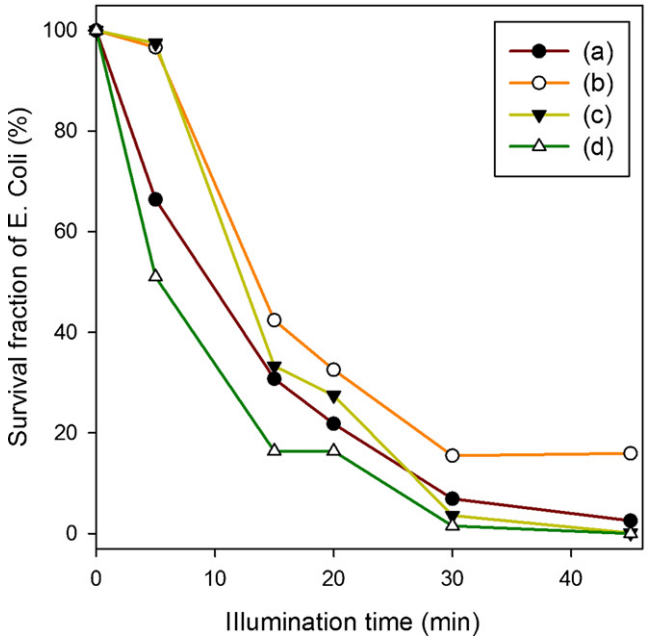

Fig. 9. Survival fraction of (a) Ag–$K_4Nb_6O_{17}$, (b) Ag–Cu(1) $K_4Nb_6O_{17}$, (c) Ag–Cu(2) $K_4Nb_6O_{17}$ and (d) Ag–Cu(3) $K_4Nb_6O_{17}$ for the photokilling of *E. coli* under visible light irradiation.

4. Conclusion

A series of novel Ag, Cu, and Ag–Cu modified $K_4Nb_6O_{17}$ films for photocatalytic inactivation of *E. coli* under visible light irradiation was prepared. We preformed the antibacterial activity test on theses photocatalyst films according to JIS Z 2801: 2000. It was found that $K_4Nb_6O_{17}$ was active for photocatalytic destruction of *E. coli* under visible light irradiation.

Our results demonstrated that highly efficient Ag–Cu/$K_4Nb_6O_{17}$ films with well dispersed Ag–Cu nanocomposites (mean particle size = 12 nm) can be synthesized by reduction of $CuSO_4$ with PVP protection, followed by impregnation $AgNO_3$ and thermal calcination. The considerable improvement was attributed to the Au–Cu nanocomposite cocatalysts efficiently suppressed the electron–hole recombination and the synergistic effects of coexisting Ag and Cu ions on antibacterial activity.

Acknowledgement

This research was supported by the National Science Council, Taiwan, Republic of China (NSC 98-2221-E-259-012-MY2).

Appendix A. Supplementary data

Supplementary data associated with this article can be found, in the online version, at doi:10.1016/j.jhazmat.2012.03.014.

References

[1] S. Josset, N. Keller, M.C. Lett, M.J. Ledoux, V. Keller, Numeration methods for targeting photoactive materials in the UV-A photocatalytic removal of microorganisms, Chem. Soc. Rev. 37 (2008) 744–755.
[2] G. Yan, J. Chen, Z. Hua, Roles of H_2O_2 and OH radical in bactericidal action of immobilized TiO_2 thin-film reactor: an ESR study, J. Photochem. Photobiol. A: Chem. 207 (2009) 153–159.
[3] A.K. Benabbou, Z. Derriche, C. Felix, P. Lejeune, C. Guillard, Photocatalytic inactivation of *Escherichia coli* – effect of concentration of TiO_2 and microorganism, nature, and intensity of UV irradiation, Appl. Catal. B 76 (2007) 257–263.

[4] A. Slominski, J. Pawelek, Animals under the sun: effects of ultraviolet radiation on mammalian skin, Clin. Dermatol. 16 (1998) 503–515.
[5] J.C. Yu, W. Ho, J. Yu, H. Yip, P.K. Wong, J. Zhao, Efficient visible-light-induced photocatalytic disinfection on sulfur-doped nanocrystalline titania, Environ. Sci. Technol. 39 (2005) 1175–1179.
[6] P.G. Wu, R.C. Xie, K. Imlay, J.K. Shang, Visible-light-induced bactericidal activity of titanium dioxide codoped with nitrogen and silver, Environ. Sci. Technol. 44 (2010) 6992–6997.
[7] I.H. Tseng, W.-C. Chang, J.C.S. Wu, Photoreduction of CO_2 using sol–gel derived titania and titania-supported copper catalysts, Appl. Catal. B: Environ. 37 (2002) 37–48.
[8] G.Q. Guan, T. Kida, T. Harada, M. Isayama, A. Yoshida, Photoreduction of carbon dioxide with water over $K_2Ti_6O_{13}$ photocatalyst combined with Cu/ZnO catalyst under concentrated sunlight, Appl. Catal. A: Gen. 249 (2003) 11–18.
[9] I.H. Tseng, J.C.S. Wu, Chemical states of metal-loaded titania in the photoreduction of CO_2, Catal. Today 97 (2004) 113–119.
[10] K. Page, R. Palgrave, I. Parkin, M. Wilson, S. Savin, A. Chadwick, Titania and silver¡Vtitania composite films on glass¡Xpotent antimicrobial coatings, J. Mater. Chem. 17 (2007) 95–104.
[11] I. Chopra, The increasing use of silver-based products as antimicrobial agents: a useful development or a cause for concern? J. Antimicrob. Chemother. 59 (2007) 587–590.
[12] Q.L. Feng, J. Wu, G.Q. Chen, F.Z. Cui, T.N. Kim, J.O. Kim, A mechanistic study of the antibacterial effect of silver ions on *Escherichia coli* and *Staphylococcus aureus*, J. Biomed. Mater. Res. 52 (2000) 662–668.
[13] D. Mara, N.J. Horan, The Handbook of Water and Wastewater Microbiology, Academic, San Diego, CA, 2003.
[14] D.Q. Zhang, G.S. Li, J.C. Yu, Inorganic materials for photocatalytic water disinfection, J. Mater. Chem. 20 (2010) 4529–4536.
[15] Z.G. Zou, J.H. Ye, K. Sayama, H. Arakawa, Direct splitting of water under visible light irradiation with an oxide semiconductor photocatalyst, Nature 414 (2001) 625.
[16] H.Y. Lin, T.H. Lee, C.Y. Sie, Photocatalytic hydrogen production with nickel oxide intercalated $K_4Nb_6O_{17}$ under visible light irradiation, Int. J. Hydrogen Energy 33 (2008) 4055–4063.
[17] M. Koinuma, H. Seki, Y. Matsumoto, Photoelectrochemical properties of layered niobate ($K_4Nb_6O_{17}$) films prepared by electrophoretic deposition, J. Electroanal. Chem. 531 (2002) 81–85.
[18] Y. Sasaki, H. Nemoto, K. Saito, A. Kudo, Solar water splitting using powdered photocatalysts driven by Z-schematic interparticle electron transfer without an electron mediator, J. Phys. Chem. C 113 (2009) 17536–17542.
[19] M. Gasperin, M.T. Le Bihan, Mecanisme d'hydratation des niobates alcalins lamellaires de formule $A_4Nb_4O_{17}$ (A = K, Rb, Cs), J. Solid State Chem. 43 (1982) 346.
[20] JIS Z 2801: 2000 (E) Antimicrobial Products, Test for Antimicrobial Activity and Efficiency, Industrial Standard, Japanese Standards Association, 2006.
[21] M.A. Bizeto, V.R.L. Constantino, Structural aspects and thermal behavior of the proton-exchanged layered niobate $K_4Nb_6O_{17}$, Mater. Res. Bull. 39 (2004) 1729–1736.
[22] J. Oi-Uchisawa, A. Obuchi, R. Enomoto, S.T. Liu, T. Nanba, S. Kushiyama, Catalytic performance of Pt supported on various metal oxides in the oxidation of carbon black, Appl. Catal. B: Environ. 26 (2000) 17–24.
[23] V. Engels, F. Benaskar, D.A. Jefferson, B.F.G. Johnson, A.E.H. Wheatley, Nanoparticulate copper – routes towards oxidative stability, Dalton Trans. 39 (2010) 6496–6502.
[24] A. Kubacka, M. Ferrer, A. Martínez-Arias, M. Fernández-García, Ag promotion of TiO_2-anatase disinfection capability: study of *Escherichia coli* inactivation, Appl. Catal. B 84 (2008) 87–93.
[25] L. Huang, F. Peng, F.S. Ohuchi, In situ XPS study of band structures at Cu_2O/TiO_2 heterojunctions interface, Surf. Sci. 603 (2009) 2825–2834.
[26] J. Yu, J. Xiong, B. Cheng, S. Liu, Fabrication and characterization of Ag–TiO_2 multiphase nanocomposite thin films with enhanced photocatalytic activity, Appl. Catal. B 60 (2005) 211–221.
[27] J.F. Moulder, J.E. Chastain, Handbook of X-ray Photoelectron Spectroscopy: A Reference Book of Standard Spectra for Identification and Interpretation of XPS Data, Perkin-Elmer Corporation, Physical Electronics Division, Eden Prairie, MN, 1992.
[28] L. Shang, B. Li, W. Dong, B. Chen, C. Li, W. Tang, G. Wang, J. Wu, Y. Ying, Heteronanostructure of Ag particle on titanate nanowire membrane with enhanced photocatalytic properties and bactericidal activities, J. Hazard. Mater. 178 (2010) 1109–1114.
[29] Y.-S.E. Lin, R.D. Vidic, J.E. Stout, V.L. Yu, Individual and combined effects of copper and silver ions on inactivation of *Legionella pneumophila*, Water Res. 30 (1996) 1905–1913.
[30] J.P. Ruparelia, A.K. Chatterjee, S.P. Duttagupta, S. Mukherji, Strain specificity in antimicrobial activity of silver and copper nanoparticles, Acta Biomater. 4 (2008) 707–716.
[31] Z. Xiong, J. Ma, W.J. Ng, T.D. Waite, X.S. Zhao, Silver-modified mesoporous TiO_2 photocatalyst for water purification, Water Res. 45 (2011) 2095–2103.
[32] A. Pal, S.O. Pehkonen, L.E. Yu, M.B. Ray, Photocatalytic inactivation of Gram-positive and Gram-negative bacteria using fluorescent light, J. Photochem. Photobiol. A 186 (2007) 335–341.
[33] K. Sunada, T. Watanabe, K. Hashimoto, Bactericidal activity of copper-deposited TiO_2 thin film under weak UV light illumination, Environ. Sci. Technol. 37 (2003) 4785–4789.